International Journal of Civil Engineering

Structure-Concrete

Investigating the resistance of alkali-activated slag mortar exposed to magnesium sulfate attack

A. Allahvedi[1, 2,*], H. Hashemi[2]

Received: May 2013, Revised: November 2014, Accepted: December 2014

Abstract

This paper presents an investigation on durability of alkali-activated slag mortar against magnesium sulfate attack. To do so, the immersion tests in 5% magnesium sulfate solution under room temperature and wetting-drying cycles were applied. Mortar specimens from Portland cements type 2 and 5 in accordance to ASTM standard were also prepared and used as reference. The changes in compressive strength and length of specimens were measured at different time intervals and considered for evaluating the extent of degradation. After 360 days of exposure to the magnesium sulfate solution, type 2 and 5 Portland cements and alkali-activated slag cement have shown 61, 41 and 34% reduction in compressive strength and 0.093, 0.057 and 0.021% increase in length, respectively. The specimens were also studied by X-ray diffractometry and scanning electron microscopy for characterizing the chemical products of the degradation process. Main degradation products were ettringite and gypsum for Portland cements and gypsum for alkali-activated slag cement. According to the obtained results, alkali-activated slag cement exhibits a higher sulfate resistance compared to type 2 and even type 5 Portland cements.

Keywords: *Magnesium sulfate, Alkali-activated slag, Compressive strength.*

1. Introduction

In the last decades, attention has increasingly been paid on alkali activated binders [1-4]. Most of the investigations done on alkali-activated binders is related to alkali-activated blast furnace slag, also known as ‘‘alkali-activated slag (AAS)’’ [5-8]. Blast furnace slag is a by-product of iron production industry, having a high content of calcium oxide and silica which are due to the use of iron ore and calcium carbonate in the iron production process [9]. This by-product is usually activated with different alkaline solutions based on combinations of alkali hydroxide and alkali silicates [8, 10]. The mechanism of alkali activation is not yet completely known, but is believed to consist of dissolution and precipitation stages followed by a solid state reaction resulting in the formation of C-S-H as the main hydration product [8,11].

AAS does not require high energy costs in its manufacturing process as compared to Portland cement (PC) [12]. Manufacture of AAS-based concrete would contribute not only to the development of a green low energy technology, but also to the development of high - performance concrete-based products.

Concrete products produced from AAS are characterized by their low heat of hydration, high mechanical strength and high sulfate and sea water resistance [13-16].

In the case of Portland cement-based concrete, the attacking sulfate ions react with hydration products. In the presence of calcium hydroxide and water, monosulfate hydrate and calcium aluminate hydrate react with attacking sulfate to produce ettringite. Gypsum, in addition to ettringite, can also be produced during sulfate attack. Formation of these products is expansive and capable for cracking and finally loss of strength [17-19]. Incorporation of suitable supplementary cementing materials such as fly ash, slag, silica fume, rice husk ash usually reduces the amount of expansion and the risk of concrete cracking [20, 21].

Very few studies, done on sulfate resistance of AAS binder, has claimed a different mode of degradation which could provide a superior durability performance in sulfate environment depending on chemical composition of the slag and its reactivity [16, 22].

This work is devoted to the resistance of AAS against magnesium sulfate attack. Both paste and mortar specimens were prepared and used in immersion tests in 5% magnesium sulfate solution under room temperature and wetting-drying cycles. The extent of degradation has been evaluated by measuring the changes in the compressive strength and length of mortar specimens. Paste specimens were also used for studies by X-ray diffractometry and scanning electron microscopy for characterizing the chemical products of the degradation process.

** Corresponding author: ali.allahverdi@iust.ac.ir*
1 Research laboratory of Inorganic Chemical Process Technologies, School of Chemical Engineering, Iran University of Science and Technology, Narmak 1684613114, Tehran, Iran
2 Cement Research Center, Iran University of Science and Technology, Narmak 1684613114, Tehran, Iran

[DOI: 10.22068/IJCE.13.4.379]

2. Experimental

2.1. Materials

Blast-furnace slag was prepared from Isfahan steel plant in Iran and ground in a laboratory ball mill to a residue of 1.5 wt% by weight on 90 micron sieve. The prepared slag was also characterized for its chemical and mineralogical compositions by wet analysis and X-ray diffractometry (XRD). The chemical composition and properties of type II (PC II) and type V (PC V) Portland cements, in accordance with ASTM standards, and slag are shown in Table 1. Fig. 1 shows the X-ray diffraction pattern of slag. As seen, the raw slag is mainly amorphous and consists of few amounts of crystalline phases including akermanite and calcite.

Table 1 Properties of Portland cements and Blast-furnace slag

Oxide composition (%)	PC[a] (II)	PC[b] (V)	Slag[c]
SiO_2	20.26	22.42	36.06
Al_2O_3	5.43	3.81	9.16
Fe_2O_3	3.87	4.20	0.70
CaO	64.96	64.90	36.91
MgO	0.48	0.08	10.21
SO_3	2.09	1.46	1.15
K_2O	0.60	0.42	0.70
Na_2O	0.27	0.22	0.48
LOI	1.95	1.61	-
TiO_2	-	-	3.50
MnO	-	-	1.46
V_2O_5	-	-	0.10
Free CaO	0.48	1.07	-
Bogue's phase composition (wt%)			
C_3S	60.51	53.65	-
C_2S	12.51	23.88	-
C_3A	7.84	2.99	-
C_4AF	11.78	12.78	-
Blaine Fineness (m^2/kg)	320	295	320

[a] Type II, Dorood cement factory, Iran
[b] Type V, Tehran cement factory, Iran
[c] Isfahan steel complex, Iran

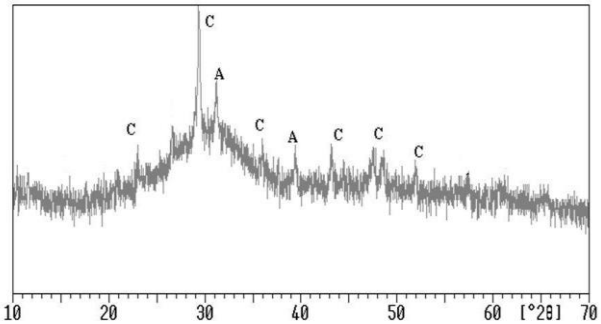

Fig. 1 X-ray diffraction pattern of slag, A=Akermanite, C=Calcite

2.2. Specimens preparation

AAS mortar and paste specimens were prepared using sodium silicate (Na_2O = 34.04 wt%, SiO_2 = 31.36 wt%, H_2O = 34.60 wt%) and sodium hydroxide (Merck company with purity grade higher than 98%) as the constituents of the activator. Standard sand (DIN-EN 196-1) was used for mortar specimens. The water-to-binder (w/b) for AAS mortar was fixed at 0.43 to obtain almost the same workability as in standard Portland cement mortar. Sodium silicate, sodium hydroxide and water were blended at given proportions to produce an alkali-activator with a silica modulus (M_s= mass ratio of SiO_2 to Na_2O) equal to 0.40, containing 2.70 wt% Na_2O by weight of slag. The sand-to-slag ratio was fixed at 2.75 to enable direct comparison with PC and to obtain reasonable mortar workability. For AAS paste specimens, the water-to-binder ratio, M_s and wt% Na_2O were adjusted at 0.26, 0.40 and 2.00, respectively. The water-to-binder ratio of fresh AAS paste was determined in accordance with ASTM C187 for achieving normal consistency. The initial and final setting times of AAS paste measured in accordance with ASTM standard C191 were 280 and 425 min, respectively.

For Portland cement mortars and pastes, water-to-binder ratios were fixed at 0.485 and 0.26 in accordance with ASTM C109 and C187, respectively. The initial and final setting times of Portland cement pastes measured in accordance with ASTM standard C191 were 120 and 180 min for PCII and 115 and 197 min for PCV, respectively. Specimens of Portland cement mortars were prepared in accordance with ASTM C109 standard. To prepare AAS mortar specimens, the prepared activator was first added to slag and mixed for 3 min and then sand was added, followed by remixing for 2 more minutes in a planetary mixer. Mortar specimens were cast for measurements of compressive strength and length changes in 50-mm cubes and 25×25×285 mm prisms, respectively. Cubic paste specimens of the size 2×2×2 cm^3 were also prepared for X-ray diffractometry and Scanning electron microscopy studies. All the molds were held at an ambient of more than 95% relative humidity for preventing drying and giving enough time (24 hours) to the pastes and mortars to set and harden at ambient temperature (25 °C). After demoulding, all the specimens were cured in tap-water until the testing time.

The pH value of the alkali-activators based on sodium hydroxide and sodium silicate are quite high and close to 14, but after completion of hydration reactions and consumption of alkali-activator the pH value of the pore solution of AAS paste decreases to lower values in the range 11.5 to 13.5 depending on the pH of the alkali-activator [23]. The chemistry and the pH value of the pore solution of alkali-activated cements are strongly related to the nature and dosage of alkali-activator and also to the characteristics of the hydration products [2, 23]. In addition, a short review of the literature clarifies the complexity of the issue and the fact that it has not been enough investigated and requires comprehensive research works. Therefore, the role of the pH value of the pore solution of AAS mortar, compared to Portland cements,

[DOI: 10.22068/IJCE.13.4.379]

requires extensive measurements and experimental works and therefore has not been considered in the scope of the present work.

2.3. Test procedure

After 28 days of curing, the mortar specimens were firstly used for compressive strength measurement. The AAS, PC II, and PC V mortar specimens exhibited 28-day compressive strength of 52, 63 and 58 MPa, respectively. All the paste and mortar specimens were then used for immersion tests. ASTM C1012 standard "test method for length change of hydraulic cement mortars exposed to a sulfate solution" was used as the basis for the sulfate resistance test. The cured specimens were immersed in a 5% magnesium sulfate solution as the aggressive environment. The temperature of the solution was kept constant at 25 °C. 12-hour cycles of wetting and drying were also applied to accelerate the rate of deterioration. The solution was renewed every week during the first 2 months, and then once after 3, 4, 5, 6, 8 and 10 months of exposure. The extent of deterioration was evaluated over a 12-month exposure time. At predetermined intervals, the specimens were tested to measure the compressive strength reduction and length changes. A total of three cubes were used for each measurement of compressive strength. The compressive strength reduction was calculated as follows:

$$\text{Compressive Strength Reduction (\%)} = [(B-A)/A] \times 100$$

Where A (in MPa) is the average compressive strength of three specimens after 28 days of curing and B (in MPa) is the average compressive strength of three specimens exposed to sulfate solution. Also, according to ASTM C 1012, length changes were calculated as follows:

$$\Delta L = [(L_x - L_i)/L_g] \times 100$$

Where ΔL is the change in length at the age of x expressed in percent, L_x is the average comparator reading of three specimens at the age of x, L_i is the average initial comparator reading of three specimens and L_g is nominal gage length. The extent of deterioration was also followed by a record of visual observations. X-ray diffraction and Scanning electron microscopy were used for identification of degradation products. To perform XRD analysis, samples were prepared and finely ground from deteriorated paste specimens. XRD analyses were performed on Siemens D500 model using Cu–Kα radiation with a voltage and ampere of 35 kV and 20 mA, respectively. Samples preparation for SEM analysis involved drying, cutting to appropriate pieces, and then coating with gold. SEM analysis in SE mode were made using TESCAN VEGA II with accelerating voltage of 20 kV.

3. Results and Discussion

3.1. Visual observations

The deteriorating effects of sulfate attack on cement-based materials usually lead in visually recognizable signs. For the case of Portland cement-based products, many observations have been reported by the researchers. For AAS-based products, however, only one observation can be found in the literature.

During the course of deterioration, the changes in the appearance of the specimens were monitored visually and photographed. Figs. 2, 3, and 4 show photos prepared from PC V, PC II, and AAS mortar specimens after 70, 140, and 280 days of exposure, respectively.

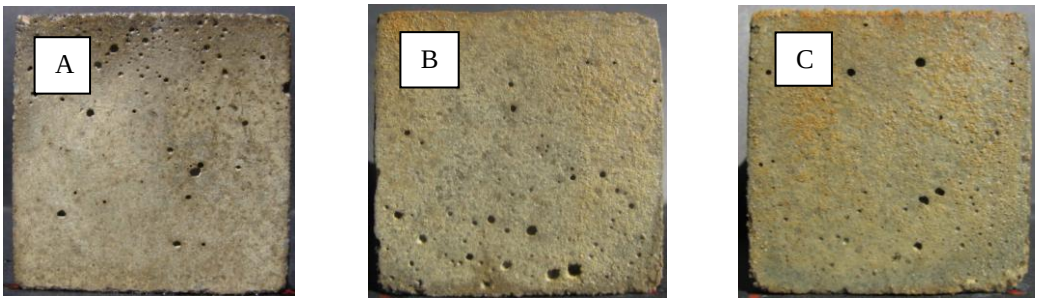

Fig. 2 PC V mortar specimens exposed to magnesium sulfate attack for A:70 days, B:140 days, C:280 days

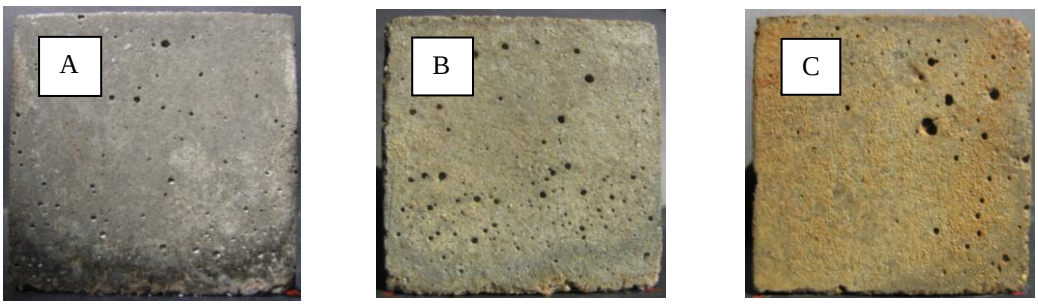

Fig. 3 PC II mortar specimens exposed to magnesium sulfate attack for A:70 days, B:140 days, C:280 days

[DOI: 10.22068/IJCE.13.4.379]

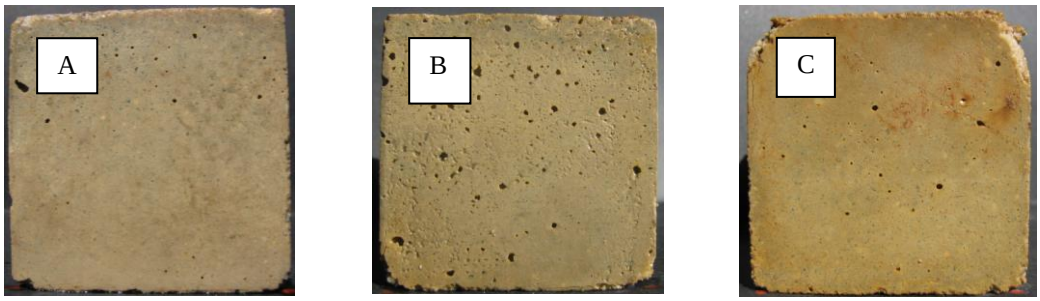

Fig. 4 AAS mortar specimens exposed to magnesium sulfate attack for A:70 days, B:140 days, C:280 days

Specimens of PC V and PC II showed no visually recognizable sign of deterioration even after 280 days of immersion. Accurate inspection of these specimens, however, showed that corners and regions close to the edges had been softened. No cracking was recognized even at the corners and regions close to the edges. AAS-specimens also retained their appearance intact until 140 days of exposure. Prolonged exposure times, however, resulted in the visual appearance of deterioration. As seen in the corresponding photo, the corners of the specimens had been destroyed due to very fine cracking and softening. No change in color was recognized except the light brown stain on some surfaces caused by the corrosion of steel net used for suspending specimens in the solution. The steel wires of the net were covered with plastic cover, but diffusion of the sulfate solution beneath the cover resulted in partial corrosion of the steel wires.

3.2. Compressive strength

The compressive strength changes of different mortar specimens exposed to magnesium sulfate solution at 25 ºC and subjected to wetting-drying cycles are shown in Fig. 5.

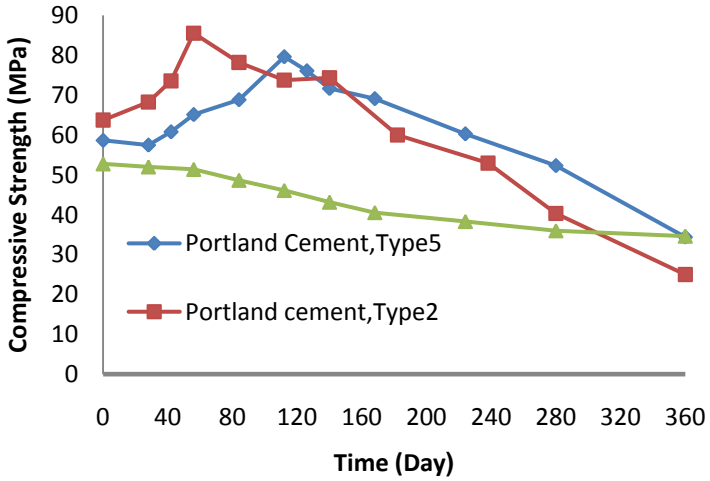

Fig. 5 Compressive strength of mortar specimens subjected to magnesium sulfate attack

As seen, specimens of PC II and PC V exhibited some increase in compressive strength until 60 and 120 days of exposure, respectively. This limited increase is due to the progress of hydration reactions inside the specimens and probably to a lesser extent to the deposition of gypsum at regions close to the exposed surfaces resulting in densification. Prolonged exposure, however, resulted in continuous strength reduction. This continuous strength reduction is believed to be due to internal disintegrating stresses exerted by the formation of voluminous compounds including gypsum and ettringite [18-19].

AAS-specimens showed a continuous strength reduction from the beginning of the exposure time with no strength increase. This pattern of strength change confirms the effective termination of the hardening reactions after 28 days of curing and the deteriorating effects of the magnesium sulfate attack from the beginning of the exposure time. Such a different behavior compared to Portland cements shows the higher vulnerability of AAS specimens during the first several months of exposure. The results obtained from continued exposure, however, showed a different situation. Accurate inspection of the strength changes after 120 days of exposure reveals significantly different strength reduction trends. The steepness of the strength reduction curves decreases in the order of PC II, PC V, and AAS, so that the residual compressive strengths after prolonged exposure times (after 360 days and later) show a different order of sulfate resistance.

To clarify the resulting conclusions, the measured compressive strengths at different time intervals were compared with the corresponding initial values (28-day compressive strengths) and the percentage of the strength reductions were calculated and presented graphically in Fig. 6.

[DOI: 10.22068/IJCE.13.4.379]

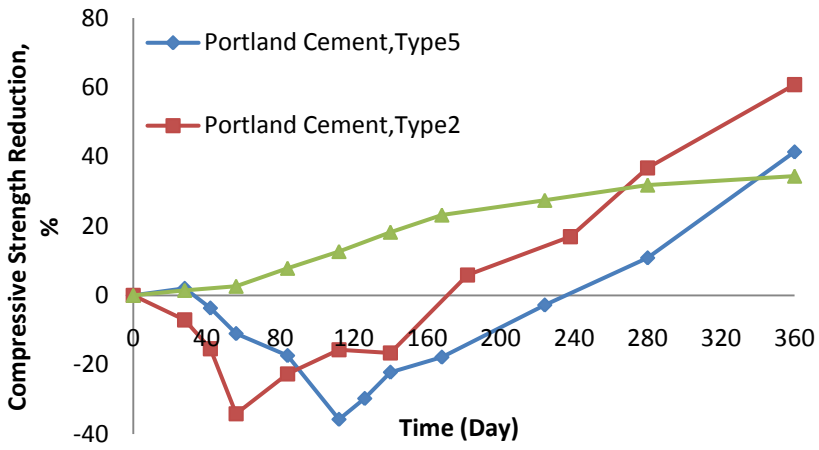

Fig. 6 Compressive strength reduction of mortar specimens subjected to magnesium sulfate attack

The strength reduction after 360 days of exposure for AAS, PC V, and PC II are 34%, 41% and 61%, respectively. All the three tested cements are more or less vulnerable to magnesium sulfate attack. The strength reductions of PC II and PC V, however, are 1.8 and 1.2 times higher than that of AAS, respectively. AAS-mortar specimens therefore exhibit a better resistance against magnesium sulfate over prolonged exposure times.

3.3. Length changes

The length changes of mortar specimens exposed to magnesium sulfate solution at 25 ºC and subjected to wetting-drying cycles are shown in Fig. 7.

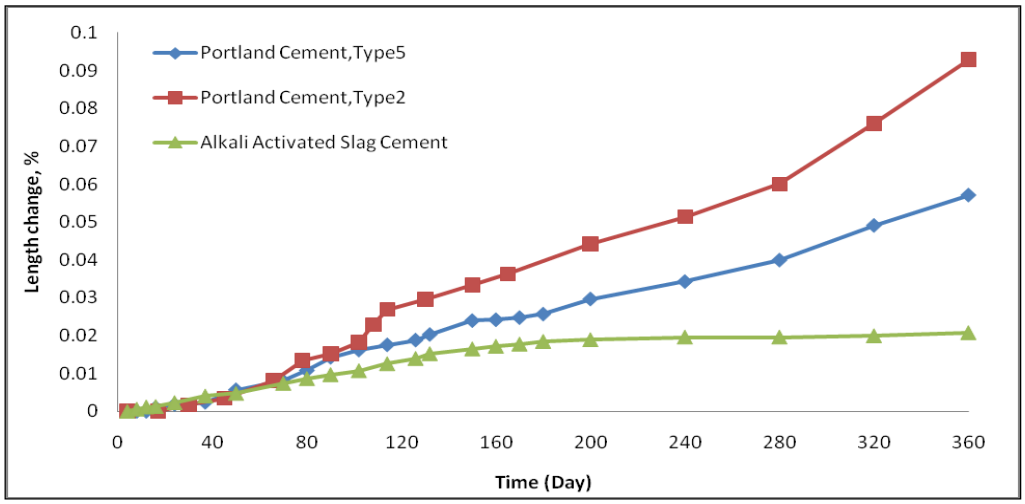

Fig. 7 Length changes of mortar specimens subjected to magnesium sulfate attack

As seen, compared to both Portland cements, AAS shows a significantly lower amount of expansion. After 360 days of exposure, AAS exhibited an expansion of only 0.021%, whereas PC V and PC II showed expansions of 0.057% and 0.093%, respectively. The higher tendency of both PC II and PC V for expansion upon magnesium sulfate attack is due to their higher capacity for formation and deposition of gypsum and ettringite in the course of expansive reactions.

3.3. X-ray diffraction

X-ray diffraction pattern of 28-day hardened paste of AAS is shown in Fig. 8. As seen, only very few weak peaks from akermanite which was originally present in the starting slag has appeared and the material exhibits a predominantly amorphous character.

[DOI: 10.22068/IJCE.13.4.379]

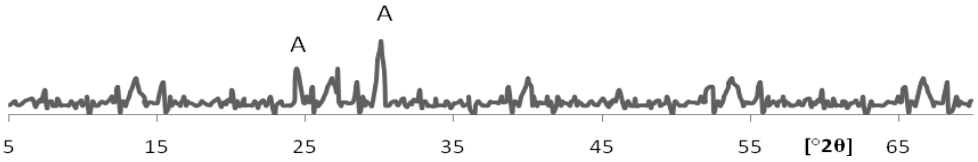

Fig. 8 X-ray diffraction pattern of alkali-activated slag, A=Akermanite

To characterize the chemical products of the degradation process, samples were also prepared and analysed from exposed paste specimens. The obtained diffraction patterns are presented in Fig. 9. As seen, after 4 months of exposure, PC samples contain considerable amounts of ettringite and gypsum, whereas AAS sample shows only few amount of gypsum with no ettringite.

Magnesium sulfate attack on hardened paste of PC is characterized by the chemical reaction of sulfate ions with calcium hydroxide and alumina-containing hydrates. The reactions between these substances produce gypsum and ettringite and causes expansion of the PC paste. At the same time, the attack of magnesium ions on C-S-H starts when CH is depleted. This attack leads to decalcification of C-S-H and gypsum deposition. The decalcification of C-S-H destroys its binding property and leads to loss of adhesion and strength. These reactions together not only cause cracking due to expansion, but also softening and disintegration due to destruction of C-S-H. Magnesium sulfate, therefore, is believed to be more aggressive than sodium sulfate [16,19].

For AAS paste, however, the experimental observations and the obtained x-ray diffraction pattern are a little bit different compared to PC pastes. As seen, the x-ray diffraction pattern of AAS paste showed no ettringite, but calcite was appeared again. The mechanism of deterioration due to magnesium sulfate attack in AAS paste is, of course, different due to its different chemical and phase compositions.

Since the original calcite was totally consumed in the alkali-activation reactions, the later appearance of calcite can be attributed to the hydration reactions of the slag. Hydration of the amorphous hydraulic phases present in slag could result in the formation of calcium hydroxide in addition to calcium-silicate hydrate. This calcium hydroxide can be slowly carbonated to calcite by reacting with atmospheric carbon dioxide. In addition, diffusion of sulfate ions into the regions close to the surfaces can also result in the formation and deposition of gypsum. Consequently, expansion and cracking of AAS paste upon sulfate attack is due to formation and deposition of gypsum and not ettringite.

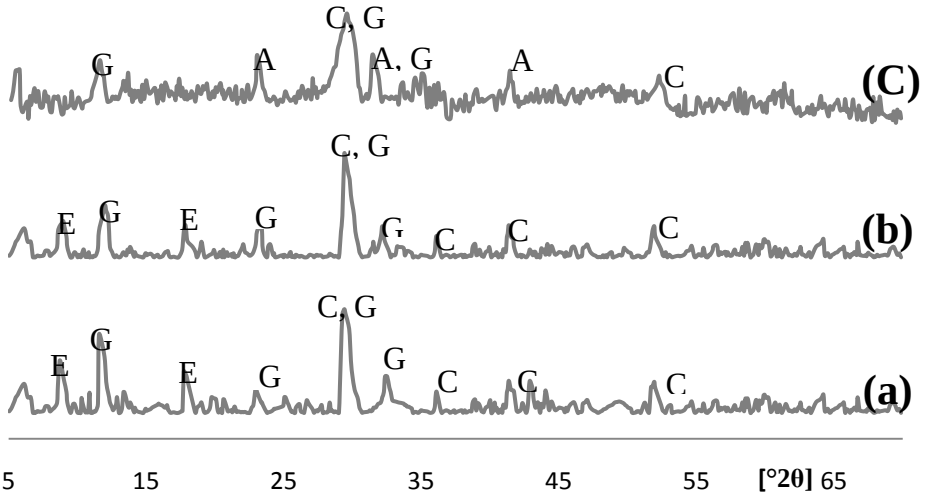

Fig. 9 X-ray diffraction patterns of paste specimens exposed to magnesium sulfate attack: (a) PC II, (b) PC V, (C) AAS, (E=Ettringite, G=Gypsum, C=Calcite, CSH= calcium silicate hydrate, A=Akermanite)

3.4. Scanning electron microscopy (SEM)

SEM images from cross sections of regions close to the exposed surfaces of the mortar specimens prepared at relatively lower magnification of 200 times are shown in Fig. 10. As seen, SEM observations revealed that magnesium sulfate attack has resulted in a loose and porous surface layer which is highly cracked. This is the soft surface layer which showed no or quite less adhesion and strength. The loss of adhesion and strength in this surface layer is due to the deteriorating action of magnesium ions on C-S-H leading to its decomposition and extensive gypsum deposition.

[DOI: 10.22068/IJCE.13.4.379]

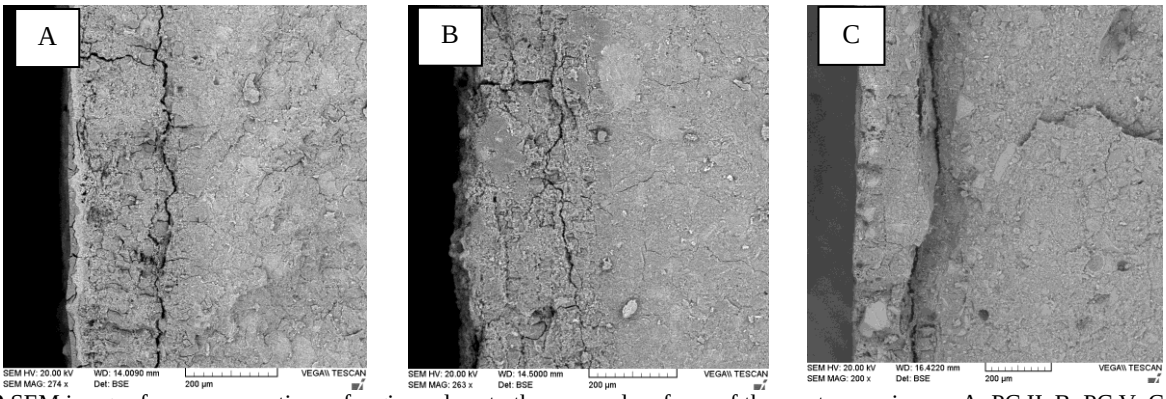

Fig. 10 SEM images from cross sections of regions close to the exposed surfaces of the mortar specimens, A: PC II, B: PC V, C: AAS

SEM observations on paste specimens confirmed extensive deposition of gypsum along with ettringite in Portland cements. Fig. 11 shows degradation products, gypsum and ettringite, observed in PC II.

Degradation products were also observed in PC V. Gypsum and ettringite crystals formed in paste specimens of PC V are shown in images A and B in Fig. 12, respectively.

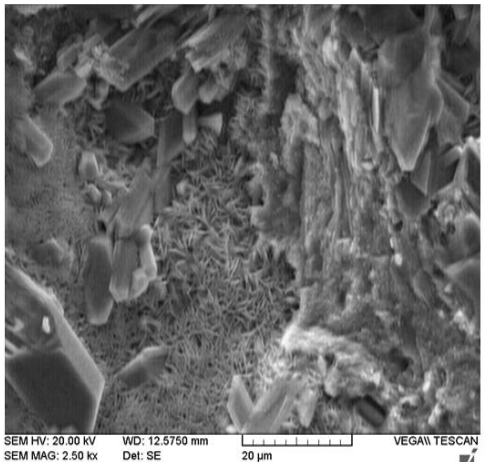

Fig. 11 SEM image from gypsum and ettringite crystals formed in paste specimens of PC II

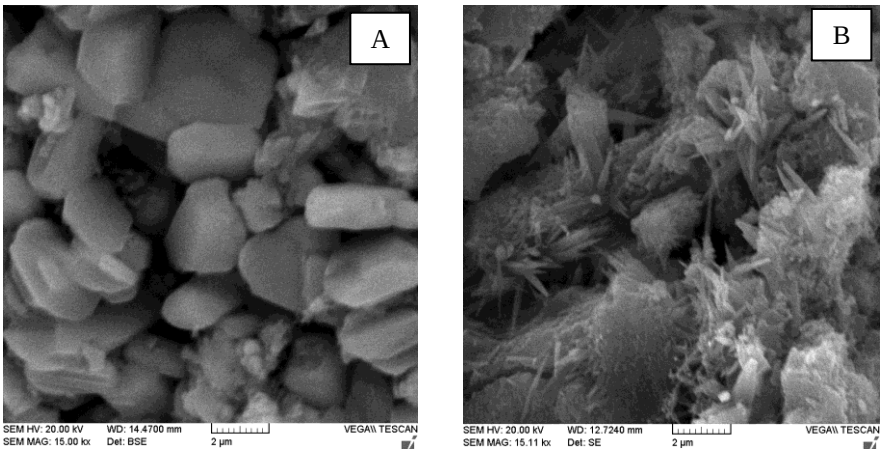

Fig. 12 SEM images of A: gypsum and B: etringite in PC V due to magnesium sulfate attack

In the case of AAS specimens, however, gypsum crystals were quite fine and highly dispersed and hence difficult to simply observe by scanning electron microscopy, although very fine micro-cracks in the paste glassy matrix at regions close to exposed surfaces were simply observable. Formation of these micro-cracks is very probably due to the increasing disintegrating expansive stresses caused by the deposition of very fine and highly dispersed gypsum crystal in the same regions. Fig. 13 represents a typical image from the same micro-cracks at a magnification of 7000 times. Continued scanning at relatively very high magnifications around micro-cracks led to the observation of very small gypsum crystal of the usual shape of hexagonal rod-like and probably the rare shape of needle-like shown in Figs. 14A and 15A, respectively. The presence of gypsum crystal in these regions can also be confirmed by the results obtained from energy

[DOI: 10.22068/IJCE.13.4.379]

dispersive X-ray spectroscopy (EDAX) technique for elemental analysis of the same crystals. As seen, the elemental spectra shown in Figs. 14B and 15B both show the presence of sulfur, calcium and oxygen as the main elements in the elemental composition of the respective crystals.

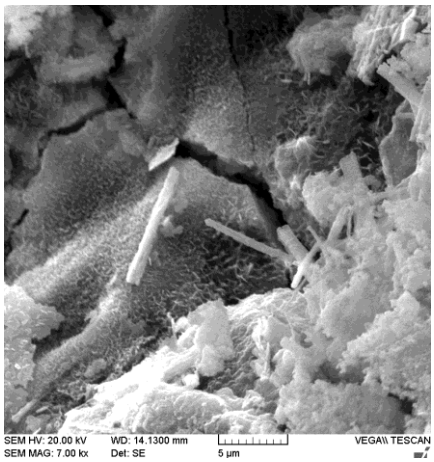

Fig. 13 SEM image from micro-cracks in AAS paste specimens exposed to magnesium sulfate attack

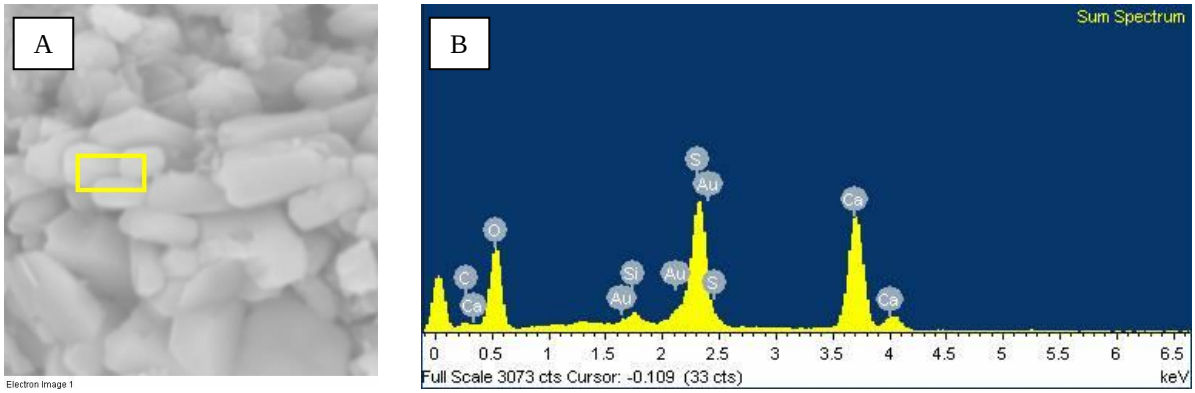

Fig. 14 EDAX elemental analysis on hexagonal rod-like crystal around micro-cracks in AAS paste specimens exposed to magnesium sulfate attack

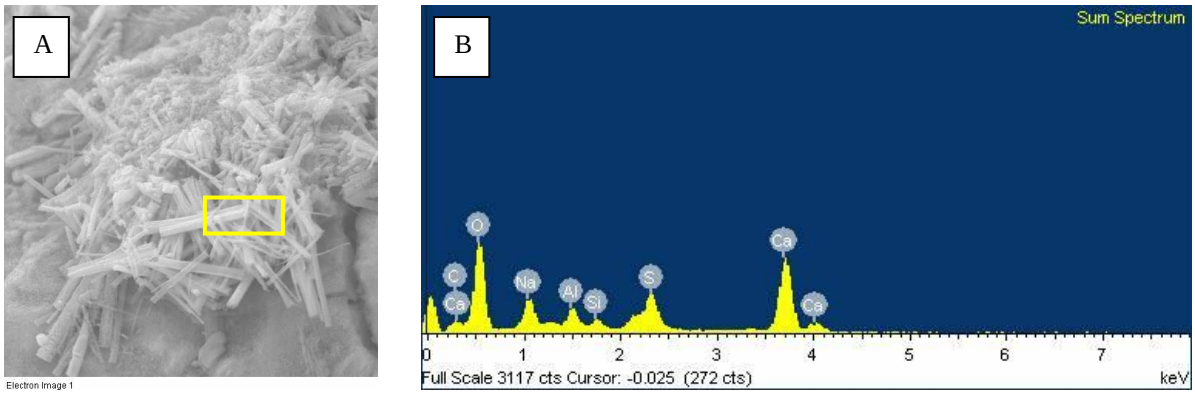

Fig. 15 EDAX elemental analysis on needle-like crystal around micro-cracks in AAS paste specimens exposed to magnesium sulfate attack

4 Conclusions

Sulfate resistance of alkali-activated slag mortar in 5% magnesium sulfate solution has been investigated and compared to type II and type V Portland cements. Mortar specimens of Portland cements showed no visually recognizable sign of deterioration even after 280 days of immersion. Accurate inspection of these specimens, however, showed that corners and regions close to the edges had been softened. Mortar specimens of alkali-activated slag also retained their appearance intact until 140 days of exposure. Prolonged exposure times, however, resulted in the visual appearance of deterioration in the form of very fine cracking, softening, and scaling at the corners. After 360 days of exposure, type 2 and 5 Portland cements and alkali-activated slag cement have shown 61, 41 and 34% reduction in compressive strength, and 0.093, 0.057 and 0.021% increase in length, respectively. Main degradation products were ettringite and gypsum for Portland cements and gypsum for alkali-activated slag

[DOI: 10.22068/IJCE.13.4.379]

cement. According to the observations and obtained results, under the tested conditions, alkali-activated slag cement exhibits a higher sulfate resistance than type 2 and even type 5 Portland cements.

References

[1] Roy DM. Alkali-activated cements; opportunities and challenges, Cement and Concrete Research, 1999, No. 2, Vol. 29, pp. 249-254.

[2] Shi C, Roy D, Krivenko P. Alkali-activated cements and concrete, Taylor & Francis Ltd, London, 2006.

[3] Fernandez-Jimenez A, Palomo J. Composition and microstructure of alkali activated fly ash binder, Effect of the activator, Cement and Concrete Research, 2005, No. 10, Vol. 35, pp. 1984-1992.

[4] Alonso S, Palomo A. Calorimetric study of alkaline activation of calcium hydroxide-metakaolin solid mixtures, Cement and Concrete Research, 2001, No. 1, Vol. 31, pp. 25-30.

[5] Purdon AO. The action of alkalis on blast furnace slag, Journal of the Society of Chemical Industry, London, 1940, Vol. 59, pp. 191-202.

[6] Caijun S, Robert D. A calorimetric study of early hydration of alkali-slag cements, Cement and Concrete Research, 1995, No. 6, Vol. 25, pp. 1333-1346.

[7] Glukhovsky VD, Rostovskaja GS, Rumyna GV. High strength slag alkaline cements, In Proceedings of the seventh international congress on the chemistry of cement, Paris, France, 1980, Vol. 3, pp. 164-168.

[8] Allahverdi A, Shaverdi B, Najafi Kani E. Influence of sodium oxide on properties of fresh and hardened paste of alkali-activated blast-Furnace slag, International Journal of Civil Engineering, 2010, No. 4, Vol. 8, pp. 304-314.

[9] Shi C, Qian J. High performance cementing materials from industrial slags- a review, Resources, Conservation and Recycling, 2000, No. 3, Vol. 29, pp. 195-207.

[10] Pacheco-Torgal F, Castro-Gomes J, Jalali S. Alkali-activated binders: A review Part 1. Historical background, terminology, reaction mechanisms and hydration products, Construction and Building Materials, 2008, No. 7, Vol. 22, pp. 1305-1314.

[11] Wang SD, Scrivener K. Hydration products of alkali activated slag cement, Cement and Concrete Research, 1995, No. 3, Vol. 25, pp. 561-571.

[12] Puertas F, Martinez-Ramirez S, Alonso S, Vasquez T. Alkali activated fly ash/slag cement and Strength behaviour and hydration products, Cement and Concrete Research, 2000, No. 19, Vol. 30, pp. 1625-1632.

[13] Pacheco - Torgal F, Castro-Gomes J, Jalali S. Alkali-activated binders: A review Part 2. About materials and binders manufacture, Construction and Building Materials, 2008, No. 7, Vol. 22, pp. 1315-1322.

[14] Glukhovsky VD. Slag-alkali concretes produced from fine-grained aggregate, Vishcha Shkolay, Kiev, Ukraine, 1981.

[15] Deng Y, Wu X, Tang M. High strength alkali-slag cement, Journal of Nanjing Institute of Chemical Technology, 1989, No. 2, Vol. 11, pp. 1-7.

[16] Bakharev T, Sanjayan JG, Cheng YB. Sulphate attack on alkali-activated slag concrete, Cement and Concrete Research, 2002, No. 2, Vol. 32, pp. 211-216.

[17] Massazza F. Pozzolanic cements, Cement Concrete Composite, 1993, No. 4, Vol. 15, pp. 185-214.

[18] Kurdowski W. Durability of blended cements in aggressive media, in: Sarkar SL, (Ed.). Mineral Admixtures in Cement and Concrete, ABI Books, 1993, Vol. 4.

[19] Young-Shik P, Jin-Kook S, Jae-Hoon L, Young-Shik S. Strength deterioration of high strength concrete in sulfate environment, Cement and Concrete Research, 1999, No. 9, Vol. 29, pp. 1397-1402.

[20] Ashrafi HR, Ramezanianpour AA. Service life prediction of silica fume concrete, International Journal of Civil Engineering, 2007, No. 3, Vol. 5, pp. 182-197.

[21] Ramezanianpour AA, Mahdi khani M, Ahmadibeni Gh. The effect of rice husk ash on mechanical properties and durability of sustainable concrete, International Journal of Civil Engineering, 2009, No. 2, Vol. 7, pp. 83-91.

[22] Bin X, Xincheng P. Study on durability of solid alkaline AAS cement, Proceeding of second International Conference, Alkaline Cement and Concrete, Kyiev, Ukraine, 1992, pp. 64-71.

[23] Song S, Jennings HM. Pore solution of alkali-activated ground granulated blast-furnace slag, Cement and Concrete Research, 1999, No. 2, Vol. 29, pp. 159-170.

[DOI: 10.22068/IJCE.13.4.379]